Proceedings World Geothermal Congress 2005
Antalya, Turkey, 24-29 April 2005

Analysis of Contemporaneous Pseudorandom Data from Two Springs in the Orakei Korako Geothermal Field of New Zealand

Jonathan D. Leaver†*, Klaus Borges†, Charles Unsworth*

†School of the Built Environment, Unitec, Private Bag 92025, Auckland, New Zealand.

*Department of Engineering Science, University of Auckland, Private Bag, Auckland, New Zealand.

jleaver@unitec.ac.nz

Keywords: Geothermal springs, signal processing, wavelets, system dynamics modelling, high sampling rate.

ABSTRACT

The Orakei Korako geothermal field in the North Island of New Zealand is an unexploited field consisting of over 30 small active geysers and about 100 hot springs. It provides an excellent opportunity to examine the naturally occurring fluctuations in geothermal surface activity. Contemporaneous measurements of conductivity, temperature, water level, barometric pressure and rainfall were collected at 5 minute intervals over a 2 month period from two springs 150 metres apart. Spectral analysis by both wavelet and Fourier transforms was used to minimise the effects of non-Gaussian signal spikes and examine spectral windows of each set of data. Analysis shows that spring fluctuations are driven predominantly by solar thermal effects with negligible influence from soli-lunar gravity tides. In addition to solar thermal tidal variations, the springs have periodic fluctuations of 11.5 minutes and 24 minutes respectively. A low barometric efficiency indicates that transmissivity in the reservoir is low. System dynamics modelling of one spring suggests that it could be driven by a low vertical flux of geothermal steam interacting with transient groundwater flow.

1. INTRODUCTION

The Orakei Korako geothermal area is located about 30 km south of Rotorua in the North Island of New Zealand. The geothermal area is about 1.8 sq. km in area and contains over thirty small active geysers and about 100 hot springs on 3 terraces. The geothermal area was substantially reduced in size in 1961 when Lake Ohakuri was formed for hydro power generation. The Lake flooded around 200 hot springs and 70 small geysers. Orakei Korako is an unexploited geothermal field and therefore provides an excellent opportunity to examine the naturally occurring fluctuations in pressure, temperature and conductivity. This study has two main purposes. The first is to identify the response of the Springs to natural forcing functions of gravitational and solar thermal tides, atmospheric pressure, and reservoir pressures. The second is to develop a simple model of one spring to explain the observed fluctuations.

2. DATA INFORMATION

2.1 Spring selection and location

Two springs, known as Springs 1 and 2, were selected for monitoring in this study. These are located on the highest level silica terrace known as the Artist's Palette (Figure 1), at an elevation of about 310 metres above mean sea level. Each Spring was about 3 metres in diameter and was suitable for accommodating the conductivity, temperature and water level instruments that required mounting on a beam spanning each Spring.

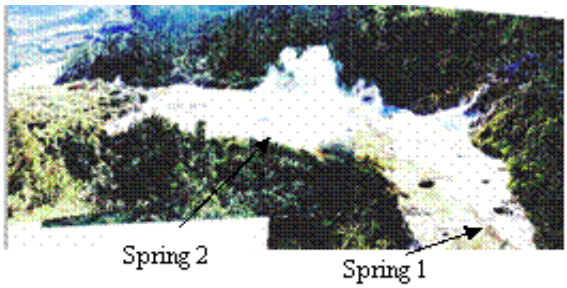

Figure 1: Aerial view of Artist's Palette

Spring 1 is located in the SE extremity of the Artist's Palette. At Spring 1, water level, conductivity and temperature were recorded. The temperature is about 80 C with a water level that varies by about 20 mm and overflows onto the surrounding silica terrace.

Spring 2 is located about 150 metres away from Spring 1 below the tourist Lookout. At Spring 2, conductivity and temperature were recorded. This spring is partially covered by trees and is characterised by vigorous boiling and low level geysering accompanied by occasional overflowing to the Artist's Palette.

Rainfall and barometric pressure were recorded at a location about midway between the two Springs.

2.2 Equipment

The data recorder used was a Unidata Blue Starlogger (www.unidata.com). The two conductivity meters consisted of a Polymetron Monec 9125 transmitter (www.polymetron.com), along with a Polymetron 8393 inductive conductivity probe. The probe has a measurement range of 0 – 2000 mS/cm, precision of ±2% or ± 0.004 mS/cm of the displayed value whichever is the greater and resolution of 0.1% of full scale. Temperatures were recorded by PT100 temperature sensors located within the Polymetron conductivity meters with a resolution of 0.005 C. Water level measurements were taken using a Unidata 6541 shaft encoder with a resolution of ±1 mm. The rain gauge was a Hydrological Services tipping bucket (www.niwa.cri.nz) with an accuracy of 15% and resolution of 1%. The atmospheric pressure sensor was a Vaisala PTB100A with accuracy ±150 Pa and repeatability of ±5 Pa.

2.3 Spring selection and location

Data collection began at 1630 hours on 4 August 2001 and continued at 5 minute intervals to 1110 hours on 4 October

2001. The data recorder was programmed to scan the instruments at 15 second intervals. Every 5 minutes the average value was recorded. The total number of data points collected was 17508 from a total monitoring time of 1458 hours and 40 minutes. In order to maintain the integrity of the data, calibration of the conductivity probes was undertaken on 10 August (142.08 - 144.67 hours); 24 August (473.00 - 473.50 hours); and 11 September (906.17 - 908.42 hours).

3. RESULTS

3.1 Barometric efficiency

The record of water level (WL), barometric pressure (BP) and rainfall is shown in Figure 2.

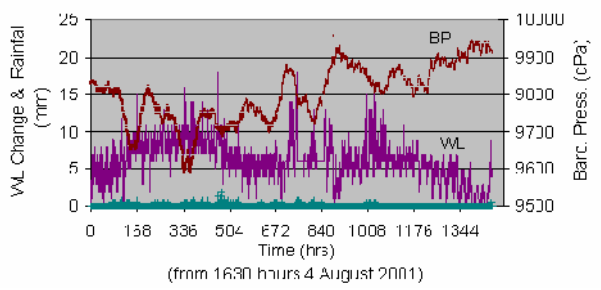

Figure 2: Barometric pressure, rainfall and water level.

The barometric efficiency, the ratio of the change in water level with barometric pressure (Bear, 1972), was calculated from water level data collected at Spring 1 from 25 September 2001 (1250 hours) to 3 October 2001 (1438 hours) as shown in Figure 3. During this period there was no rainfall, thus eliminating it as a cause of the short term fluctuations shown in Figure 3.

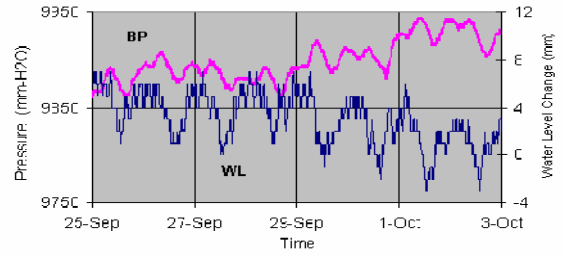

Figure 3: Barometric pressure and water level during a period of no rainfall.

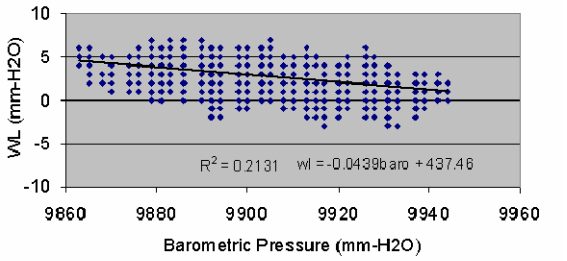

Figure 4: Variation in water level with barometric pressure

The barometric efficiency (Figure 4) is 4.4% with a linear regression R^2 value of 0.21. The low R^2 value means that the atmospheric pressure has a negligible effect on the springs.

3.2 Rainfall effects on water level

The rainfall record is shown in Figure 5.

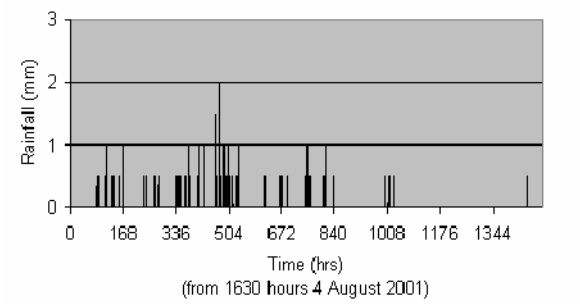

Figure 5: Rainfall record.

The effect of surface rainfall on the water level at Spring 1 was determined by first removing very low frequency components from the original water level signal. These components are likely to be caused by the transient effects of groundwater permeating into the vicinity of Spring 1 perhaps from considerable distance. This very low frequency component was removed by dividing the signal into two parts and fitting separate 5th order polynomials to each part. The polynomials were then subtracted from the raw signal (Figure 6). A polynomial correction was preferred as no data was lost due to edge effects and the integrity of data at all but the lowest frequencies was preserved.

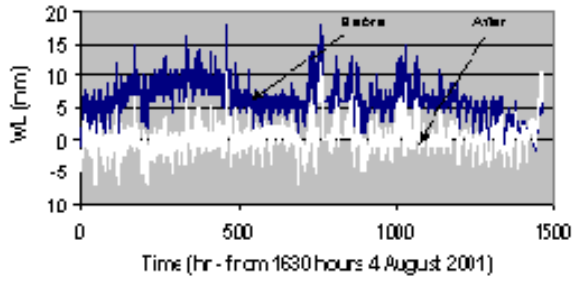

Figure 6: Comparison of the water level signal before and after polynomial correction.

Following removal of low frequency components, the water level response for the period of no rainfall from 1292.417 (1255 hours 27 August 2001) to 1413.250 (1345 hours 2 October 2001) hours was selected. The minima in this signal, which is similar to Figure 3, showed a diurnal (daily) variation with increasing period consistent with the seasonal increase in the length of a day during the spring season of the monitoring programme. The variation in period is shown in Figure 7.

The correlation between the time difference of the minima and real time is:

$$\Delta T = -0.0079 * t + 10.5 \qquad (1)$$

where ΔT = time difference (h), t = real time (h)

This correlation was used to generate an artificial signal (Figure 8) over the full length of the monitoring period, including times when there was rainfall.

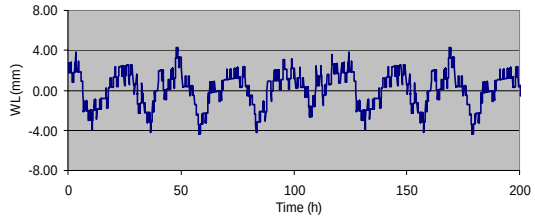

Figure 8: Artificial water level signal for no-rain conditions.

From Equation 1 the time scale for the artificial signal was adjusted by 0.79% to ensure that the minima for the artificial and real signals matched. Then the artificial signal (Figure 8) representing the water level response during a period of no rainfall was subtracted from the actual signal leaving a residual signal that should reflect any effects of rainfall (Figure 9).

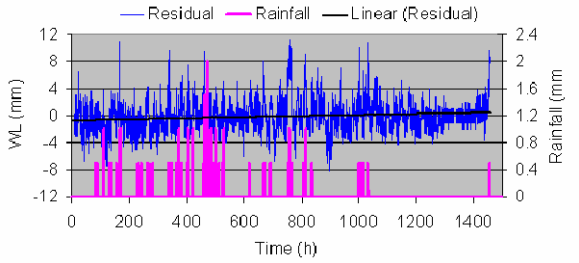

Figure 9: Rainfall and residual water level, Spring 1.

The ratio of rainfall to rise to maximum rise in the water level of Spring 1 is shown in Figure 10.

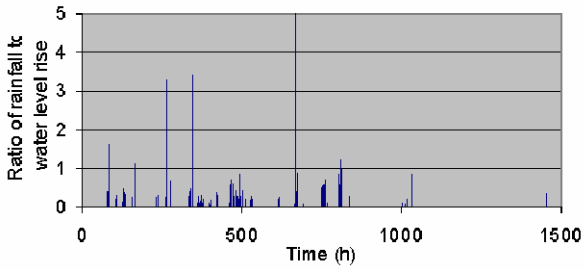

Figure 10: Variation in water level at Spring 1 with rainfall.

The ratio ranges from 0.2 to over 5 with an average of 0.4. The ratio of the rainfall peaks to water level rise is over 3 at times of 336 hours, 492 hours, and 752 hours. This is consistent with sharp reductions of over 3 C in the temperature record at times of 348 hours, 498 hours and 761 hours. Significant reductions in the temperature record also occur at other times such as 384 hours which have a lower effect on the water level. This is likely due to the different intensity profile of the rainfall and warrants further study.

The fact that the water level of Spring 1 is affected nearly instantaneously by rainfall indicates that the influence of any reservoir pressure on water level is weak. This is consistent with the low barometric efficiency and infers low vertical permeability in the connection with the underlying geothermal resource.

3.3 Characteristic periods

The temperature, conductivity and water level data collected at Spring 1; temperature and conductivity data from Spring 2, and the barometric pressure data were analysed to identify characteristic periods that could be due to soli-lunar gravity tides shown in Table 1 (Pawlowicz et al, 2002), diurnal solar thermal tides or possibly dynamic reservoir activity.

Table 1. Principal soli-lunar tide periods and amplitude ratios.

Name	Period (h)	Amp Ratio	Description	Freq
M2	12.42	1.00	Principal lunar	Semi-diurnal
K1	23.93	0.92	Lunar solar diurnal	Diurnal
O1	25.82	0.65	Principal lunar diurnal	Diurnal
S2	12.00	0.47	Principal Solar	Semi-diurnal
P1	24.07	0.30	Principal solar diurnal	Diurnal
N2	12.66	0.19	Larger lunar ellipse	Semi-diurnal

In order to determine characteristic periods analysis was undertaken firstly using Fourier transform (F method) alone and secondly using a combination of wavelet transform and Fourier transform (W-F method) (Leaver et al, 1999). A 12 level (or scale) decomposition using a “coif5” wavelet transform (Coifman and Wickerhauser, 1992) was used so that a window of the signal at the wavelet level of interest could be selected and then subjected to spectral analysis by Fourier transform. Amplitudes derived from Fourier analysis are “normalised” to the same scale as the measured values.

Analysis was focused on that part of the signal with characteristic periods of less than about 26 hours. Characteristic periods are evident at periods greater than this however the forcing functions at these lower frequencies are likely to include relatively long groundwater transients, atmospheric temperature and humidity fluctuations, and lunar fortnightly and monthly gravity effects. A long term study of characteristic fluctuations at periods greater than 26 hours is warranted but is outside the scope of this paper.

The absence in the spectral analysis of any periodic fluctuations that should be detectable at periods corresponding to the soli-lunar gravity tides M2 (12.42 hours) or O1 (25.82 hours) will be evidence that the primary drivers are solar thermal tides not gravitational tides.

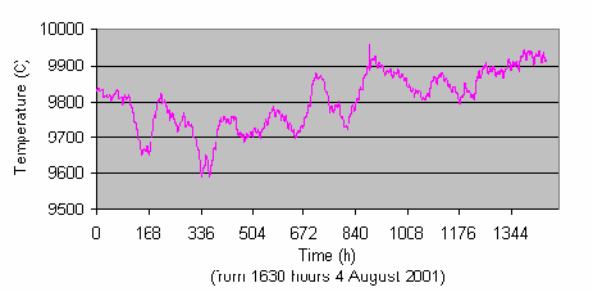

Figure 11: Barometric pressure record.

3.3.1 Analysis of Barometric Pressure

Barometric pressure data are shown in Figure 11.

Dominant periods of barometric pressure with amplitudes greater than 0.1 mm-H_2O, along with signal to noise ratios (SNR) determined from the analyses using Fourier (Figure 12) and wavelet plus Fourier transforms (Figures 13 and 14) are summarised in Table 2.

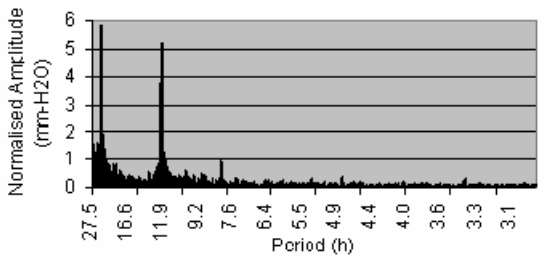

Figure 12: Periodogram of barometric pressure using analysis by Fourier transform.

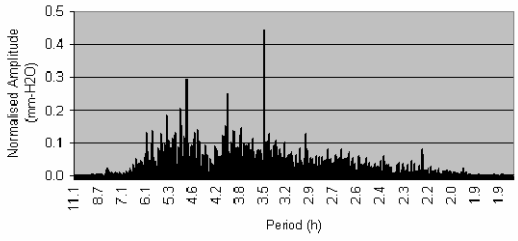

Figure 13: Periodogram of level 3 Detail of barometric pressure using analysis by wavelet and Fourier transform.

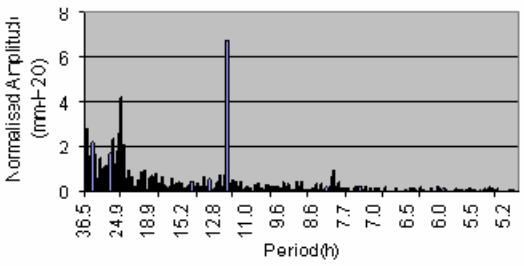

Figure 14: Periodogram of levels 6 - 8 Details of barometric pressure using analysis by wavelet and Fourier transform.

From Table 2 the dominant periods are those of the solar thermal tides at 12 hour and 24 hours with the amplitudes of the fluctuations averaged between the two methods of analysis being 5 mm-H_2O in each case. Fluctuations are also evident at other periods with those at 3.4 hours, 4.8 hours and 8.0 hours identified from both methods of analysis

Table 2. Dominant periods of barometric pressure.

W-F method			F method		
Period (h)	**Amp**	**SNR**	**Period (h)**	**Amp**	**SNR**
3.43	0.44	5	3.42	0.33	2
3.98	0.25	3			
4.79	0.30	4	4.80	0.41	3
7.98	1.00	3	5.32	0.33	2
8.04	0.64	2	8.02	0.93	3
12.00	6.79	10	11.96	5.23	3
12.04	4.69	10	12.06	3.75	3
23.70	4.17	8	23.91	5.84	3

3.3.2. Analysis of Conductivity Measurements

The conductivity data for Springs 1 and 2 are shown in Figure 15.

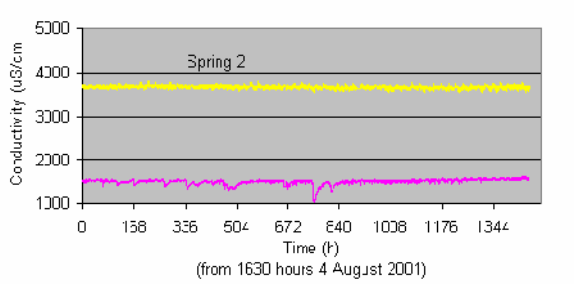

Figure 15: Conductivity of Springs 1 and 2.

The sharp drop in both conductivity and temperature in Spring 1 at 760 hours is due to the dilution effect of rainfall on the geothermal fluids. There is no evidence that the rainfall similarly affected Spring 2 that overflows at about 24 minute (Table 3) intervals and is partially covered by small trees limiting the surface catchment for rainfall.

Periodograms for Spring 1 using Fourier transform only and both wavelet and Fourier transforms are shown in Figures 16 - 18.

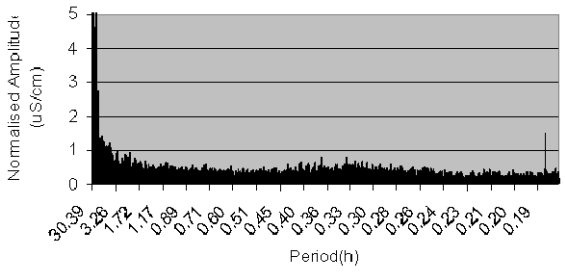

Figure 16: Periodogram of conductivity of Spring 1 using analysis by Fourier transform.

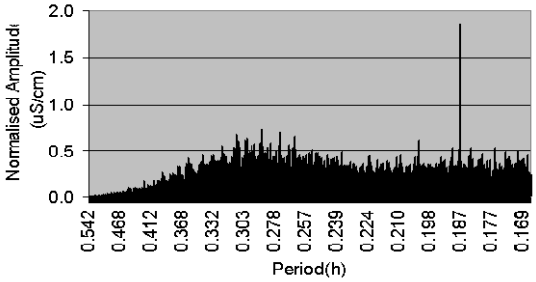

Figure 17: Periodogram of level 1 Detail of conductivity of Spring 1 using analysis by wavelet and Fourier transform.

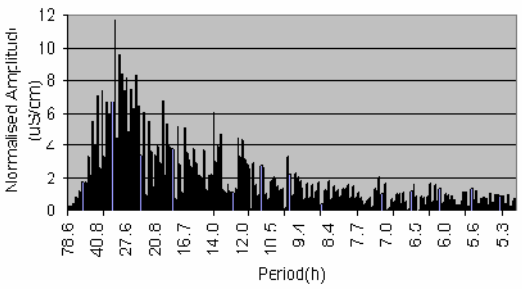

Figure 18: Periodogram of levels 6 - 8 Details of conductivity of Spring 1 using analysis by wavelet and Fourier transform.

The periodograms for Spring 2 using Fourier transform only and both wavelet and Fourier transforms are shown in Figures 19 and 20. Results are summarised in Table 3.

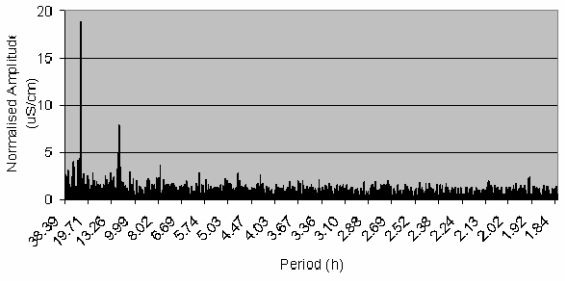

Figure 19: Periodogram of conductivity of Spring 2 using analysis by Fourier transform.

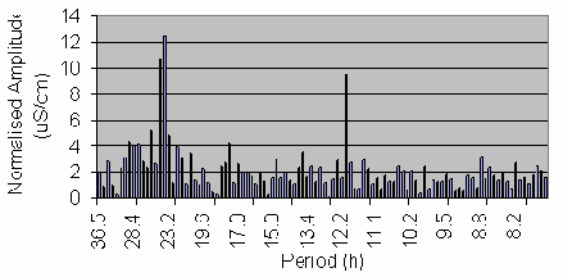

Figure 20: Periodograms of levels 6 - 8 Details of conductivity of Spring 2 using analysis by wavelet and Fourier transform.

In Spring 1 a significant characteristic oscillation is evident at a period of 0.19 hours. In Spring 2 diurnal (24 hour) and semi-diurnal (12 hour) solar thermal fluctuations are evident.

Table 3. Dominant periods of conductivity.

W-F method			F method		
Conductivity Spring 1					
Period (h)	**Amp**	**SNR**	**Period (h)**	**Amp (uS/cm)**	**SNR**
0.19	1.86	4	0.19	1.51	4
Conductivity Spring 2					
Period (h)	**Amp**	**SNR**	**Period (h)**	**Amp (uS/cm)**	**SNR**
12.01	9.56	4	11.96	7.9	2.2
23.7	12.4	5	23.91	18.9	6
24.3	10.7	5			

3.3.3 Analysis of Temperature Measurements.

Temperature data for Springs 1 and 2 are shown in Figure 21.

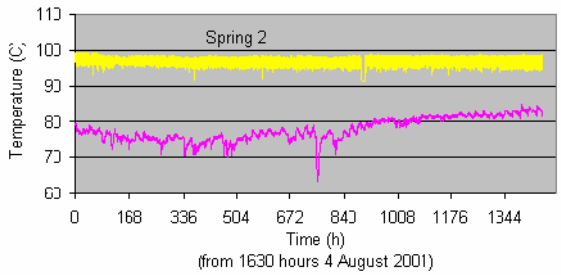

Figure 21: Temperature of Springs 1 and 2.

Periodograms for Spring 1 using Fourier transform only and both wavelet and Fourier transforms are shown in Figures 22 and 23.

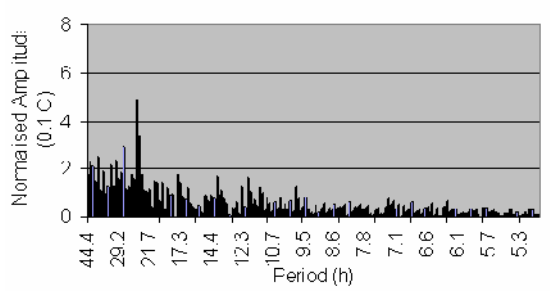

Figure 22: Periodogram of temperature of Spring 1 using analysis by Fourier transform.

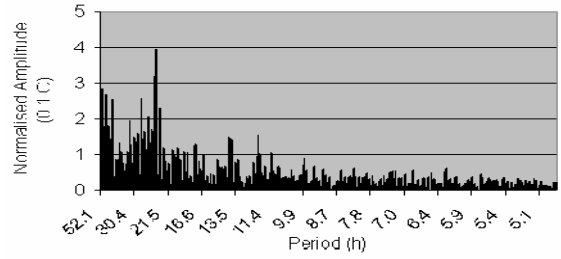

Figure 23: Periodogram of levels 6 - 8 Details of temperature of Spring 1 using analysis by wavelet and Fourier transform.

The periodograms for Spring 2 developed using both wavelet and Fourier transforms are shown in Figures 24 and 25. The results are summarised in Table 4.

In Spring 1 diurnal and semi-diurnal solar thermal tides are again evident.

3.3.4 Water level

The water level data for Spring 1 are shown in Figure 26.

A periodogram developed for the full water level signal at Spring 1 using Fourier transform only is shown in Figure 27. The periodogram for Spring 1 developed using both wavelet and Fourier transforms is shown in Figures 28. The results are summarised in Table 5.

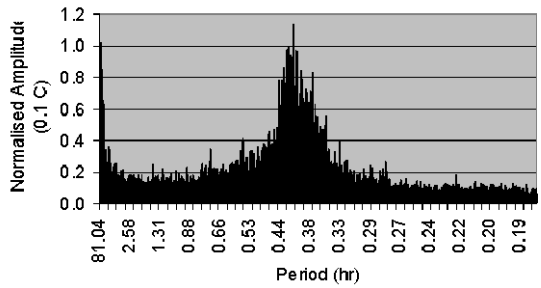

Figure 24: Periodogram of temperature of Spring 2 using analysis by Fourier transform.

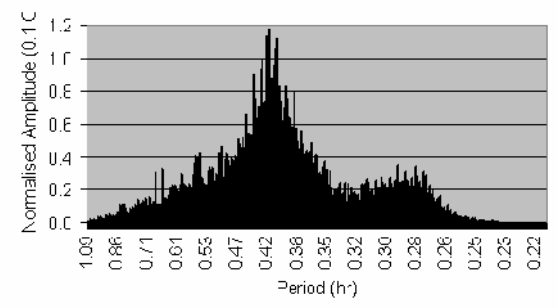

Figure 25: Periodogram of level 3 Details of temperature of Spring 2 using analysis by wavelet and Fourier transform.

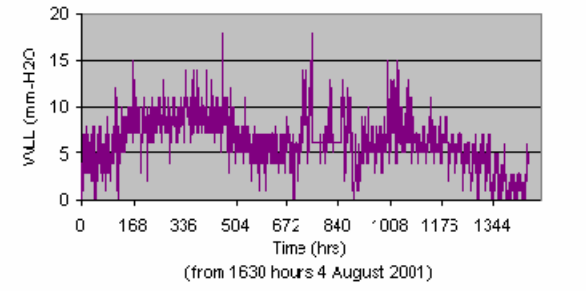

Figure 26: Water level at Spring 1.

Table 4: Dominant periods of temperature.

W-F method			F method		
Temperature Spring 1					
Period (h)	**Amp (C)**	SNR	**Period (h)**	**Amp (C)**	**SNR**
9.82	1.27	2	9.79	0.882	2
12.01	1.63	2	12.06	1.56	2
13.99	1.69	2	13.89	1.44	2
			14.03	1.48	3
17.61	1.76	2	17.37	1.29	3
23.75	3.42	3	23.91	3.94	3
24.31	4.9	4	24.31	3.18	2
Temperature Spring 2					
Period (h)	**Amp (C)**	**SNR**	**Period (h)**	**Amp (C)**	**SNR**
0.39 - 0.44	0.1	4	0.37- 0.44	0.1	4

*From level 8 Details not shown.

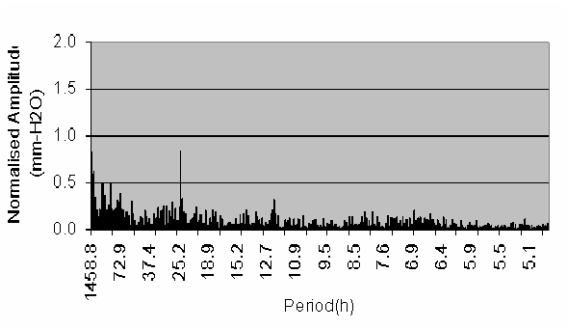

Figure 27: Periodogram of water level of Spring 1 using analysis by Fourier transform.

3.3.5 Results of Wavelet and Fourier Analysis

A summary of data from the wavelet and Fourier analysis is shown in Table 6. The absence of significant periodic fluctuations at periods typical of M2 or O1 (Table 1) is evidence that the primary drivers at diurnal and semi-diurnal periods are solar thermal tides.

The amplitude of the characteristic periodic fluctuations is generally less than 1% of the measured values for temperature and conductivity. Signal to noise ratios for the fluctuations range from 2 to 10.

The semi-diurnal amplitudes for temperature and conductivity falls are of the order of 50% of the diurnal amplitude. This is possibly due to convective heat losses causing a larger diurnal variation.

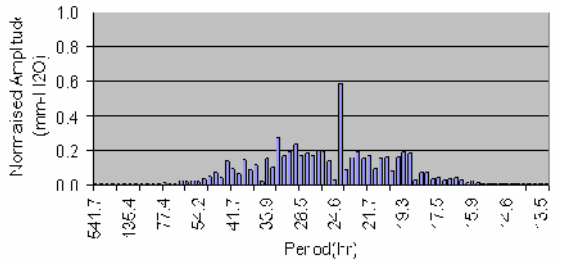

Figure 28: Periodogram of level 8 Details of water level at Spring 1 using analysis by wavelet and Fourier transform.

Table 5: Dominant periods of water level of Spring 1.

W-F method			F method		
Period (h)	**Amp (mm)**	**SNR**	**Period (h)**	**Amp (mm)**	**SNR**
			12.16	0.32	2
24.07	0.59	3	24.72	0.83	2.5

In addition to diurnal and semi diurnal fluctuations in Spring 1, significant fluctuations also occur at periods of 9.82 hours, 13.99 hours and 17.61 hours. These fluctuations may be driven by subsurface dynamics as these periods do not correspond to those exhibited by any of the other forcing functions.

In Spring 2, the lack of characteristic fluctuations in temperature is due to boiling point temperatures. Also fluctuations at about 0.4 hours (24 minutes) correspond to observed on-site water level fluctuations of up to 300 mm at the same period.

4. SYSTEM DYNAMICS MODELLING

In order to simulate the dynamics of Spring 1 at Orakei Korako a system dynamics (SD) model was developed (Figure 30). The model is designed to match the temperature record for Spring 1. It uses simulated inputs from a combination of deep geothermal steam, rainfall and shallow groundwater. In the model deep geothermal fluid assumed to be steam of enthalpy 2700 kJ/kg mixes with groundwater and rainwater. The rate of steam inflow is a function of the Spring water level. Inflows conform to a normal distribution. The groundwater has a 20 hour retention time as it is assumed to be derived from rainfall filtering through the vadose zone. The water level is constrained to simulate the elevation of Spring 1 overflows. A more detailed description of the model is planned for a subsequent paper.

A comparison of the measured and modelled temperature profile of Spring 1 in which the temperature record for Spring 1 was able to be closely replicated is shown in Figure 29.

Table 6: A summary of data from the wavelet and Fourier analysis.

W-F method			F method		
Temperature Spring 1					
Period	**Amp**	**SNR**	**Period**	**Amp**	**SNR**
9.82	1.27	2	9.79	0.882	2
12.01	1.63	2	12.06	1.56	2
13.99	1.69	2	13.89	1.44	2
			14.03	1.48	3
17.61	1.76	2	17.37	1.29	3
23.75	3.42	3	23.91	3.94	3
24.31	4.9	4	24.31	3.18	2
Temperature Spring 2					
Period	**Amp**	**SNR**	**Period**	**Amp**	**SNR**
0.39 -	0.10	4	0.37-	0.10	4
Conductivity Spring 1					
Period	**Amp**	**SNR**	**Period**	**Amp**	**SNR**
0.19	1.86	3.5	0.19	1.51	3.5
Conductivity Spring 2					
Period	**Amp**	**SNR**	**Period**	**Amp**	**SNR**
12.01	9.56	4	11.96	7.9	2.2
23.7	12.4	5	23.91	18.9	6
24.3	10.7	5			
Barometric Pressure					
Period	**Amp**	**SNR**	**Period**	**Amp**	**SNR**
3.43	0.44	5	3.42	0.33	2
3.98	0.25	3			
4.79	0.30	4	4.80	0.41	3
7.98	1.00	3	5.32	0.33	2
8.04	0.64	2	8.02	0.93	3
12.00	6.79	10	11.96	5.23	3
12.04	4.69	10	12.06	3.75	3
23.70	4.17	8	23.91	5.84	3
WL					
Period	**Amp**	**SNR**	**Period**	**Amp**	**SNR**
			12.16	0.32	2
24.07	0.59	3	24.72	0.83	2.5

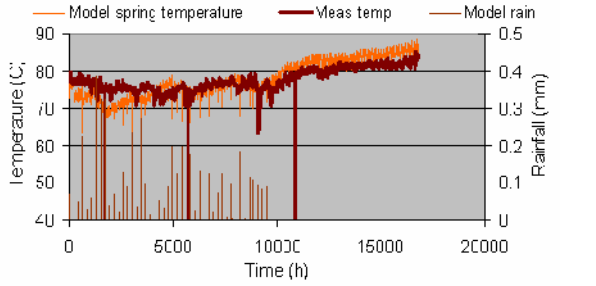

Figure 29: Comparison of modelled temperature with measured temperature.

A snapshot of typical parameters during a period of no rainfall is shown in Table 7.

Table 7: Model parameters providing match of temperature to measured values.

Parameter	Value
Spring volume	5 m^3
Deep geothermal enthalpy	2700 kJ/kg
Deep geothermal steam inflow	0.2 kg/h
Groundwater inflow	27 kg/h
Groundwater residence time	20 h

CONCLUSIONS

The key points of this study are:

- High resolution and high frequency measurements can provide very useful data in benchmarking the behaviour of surface features and therefore identifying at very early times any changes in characteristics.
- Wavelet transforms can enhance the robustness of spectral analysis by providing an alternative spectral windowing technique in the time domain from which the spectrum obtained is not subject to distortion by high energy peaks as can occur with Fourier analysis.
- Analysis of data from two springs in the Orakei Korako geothermal field confirms that fluctuations in temperature and conductivity are driven by a combination of solar thermal and dynamic reservoir processes. Springs 1 and 2 have periodic fluctuations in temperature and conductivity at periods of 11.5 minutes and 24 minutes respectively. A low barometric efficiency of 4.4% at Spring 1 indicates that, as the phase and amplitude of the reservoir response is relatively insenstive to specific storage (Narasimhan et al., 1984), it is probable that the transmissivity in the reservoir is low at that point, although it is possible that the absolute value of specific storage is also low.
- System dynamics modelling of Spring 1 shows it could be driven by a low vertical flux of geothermal steam interacting with transient groundwater flow and rainfall.

ACKNOWLEDGEMENTS

The authors gratefully acknowledge the assistance of Dr Arnold Watson, Department of Mechanical Engineering, University of Auckland, for initiating and directing this study; and the staff of the Orakei Korako Geyserland Resort in the collection of data. Funding was provided by the University of Auckland.

REFERENCES

Bear, J.: Dynamics of Fluids in Porous Media. Dover Publications. Inc. (1972).

Coifman, R.R., Wickerhauser, M.V.: Entropy-based Algorithms for Best Basis Selection. *IEEE Trans. On Inf. Theory*, **38-2**, (1992), 713 – 718.

High Performance Systems.: An Introduction to Systems Thinking. HPS Inc., New Hampshire (1994).

Leaver, J.D., Watson, A., Ding, J.J.: Application of Fourier and Wavelet Analyses to Pressure Data from the Te Aroha Hydrothermal System, *Proc. 21st N.Z. Geothermal Workshop* (1999), 211-216.

Narasimhan, T. N., Kanehiro, B. Y., Witherspoon, P. A.: Interpretation of Earth Tide Response of Three Deep, Confined Aquifers, *Journal of Geophysical Research*, **89-B3**, (1984), 1913-1924.

Pawlowicz, R., Beardsley, B., Lentz S.: Classical Tidal Harmonic Analysis including Error Estimates in MATLAB using T_TIDE. *Computers and Geosciences*, **28**, (2002), 929-937, .

The MathWorks.: MATLAB The Language of Technical Computing. MathWorks (1998).

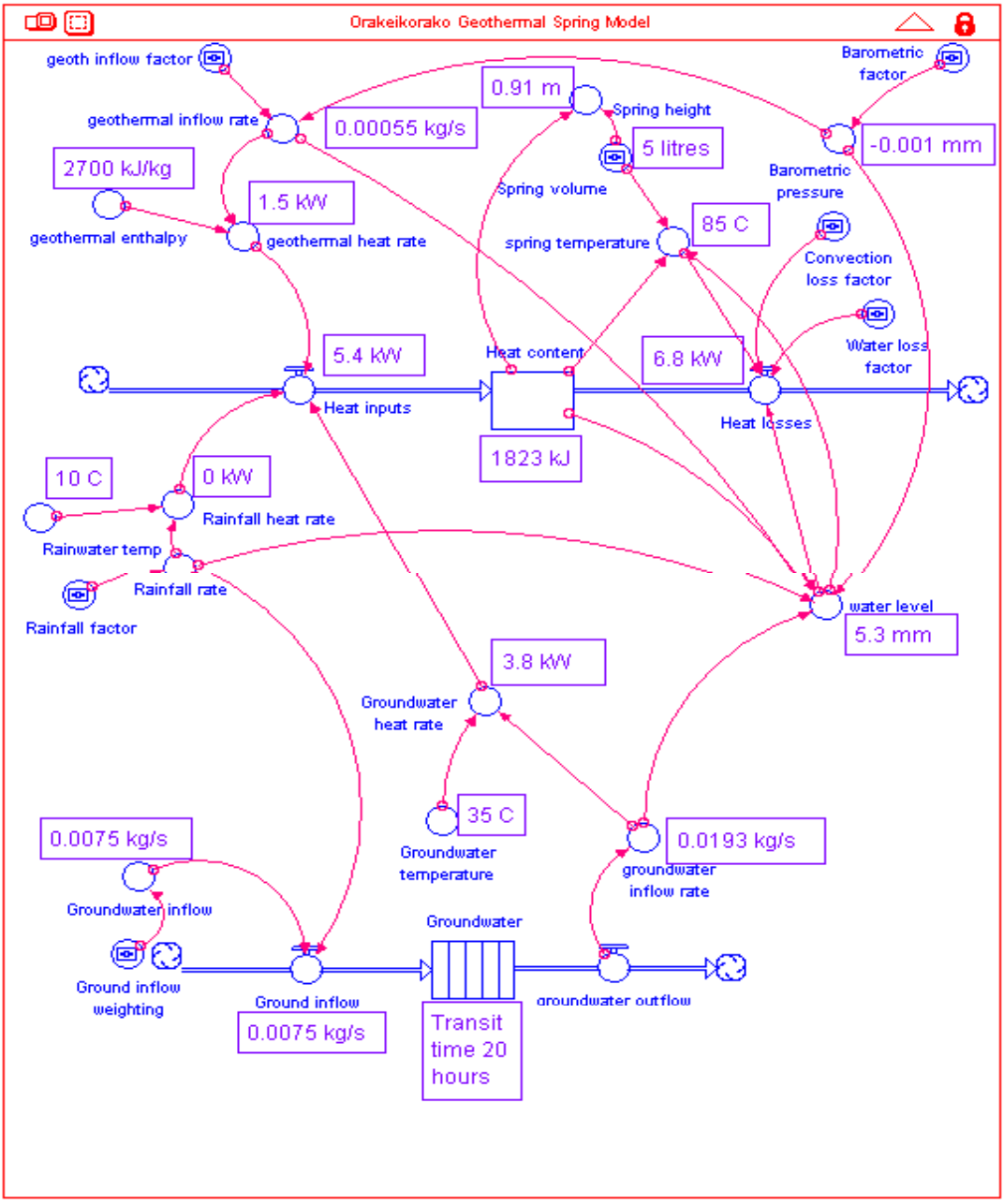

Figure 30: Network simulation for Spring 1 at Orakei Korako.